

Supplementary Information

Inducing microscopic thermal lesions for the dissection of functional cell networks on a chip.

Philipp Rinklin^a, Dzmitry Afanasekau^b, Simone Wiegand^b, Andreas Offenhäusser^{a,c}, Bernhard Wolfrum^{a,c}

^a Institute of Bioelectronics (ICS-8/PGI-8), Forschungszentrum Jülich and JARA - Fundamentals of Future Information Technology, Forschungszentrum Jülich, 52425 Jülich, Germany

^b Institute of Complex Systems - 3 - Soft Condensed Matter, Forschungszentrum Jülich, 52428 Jülich, Germany

^c IV. Institute of Physics, RWTH Aachen University, 52076 Aachen, Germany

1. Ca²⁺ propagation analysis

In order to determine the activity in the Ca²⁺ imaging, the data were processed as follows: The corresponding image stream was first downsampled to 32x32 pixels for reasons of resolution and processing speed. The downsampled image streams were then normalized by calculating $I_{norm} = (I - \bar{I})/\bar{I}$ where I_{norm} represents the normalized intensity, I the individual pixel's intensity at the given frame and \bar{I} its average intensity over time. In order to discriminate active from inactive pixels, $(I_{norm}^{-4})^{1/4}$ was calculated. Figure S1a shows the $(I_{norm}^{-4})^{1/4}$ -matrix for the video analyzed in Figures 4c and 5. Pixels with strong variations in their intensity appear bright, while pixels with less variation in their intensity appear dark. This matrix was converted to a logical mask

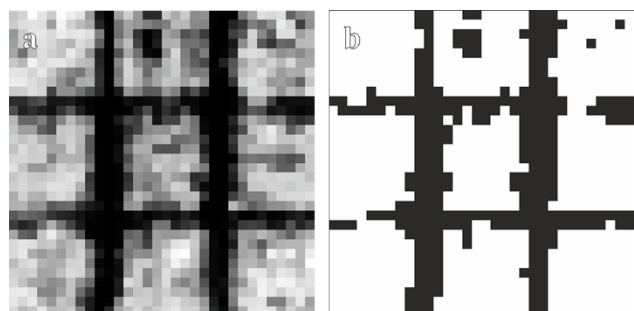


Figure S1: Determining the active areas in the Ca²⁺ imaging

videos. (a) $(I_{norm}^{-4})^{1/4}$ -matrix of the Ca²⁺ imaging sequence analyzed in Figures 4c and 5. (b) Thresholded activity mask for the same video.

using its minimum plus two times its standard deviation as a threshold. The resulting activity mask is shown in Figure S1b. This activity mask was then scanned for connected regions (i.e. regions that consist of only active pixels but are fully separated from other parts by inactive pixels). For the following correlation analyses, the intensity traces of all pixels were smoothed using a Gaussian filter with a width of 300 ms. To determine the signal's propagation inside of each region, all pixels in the region were cross-correlated with the average intensity trace of the corresponding region. Figure S2a displays the resulting delay matrix shifted to a minimum delay of 0 ms. In order to evaluate the propagation in between the individual regions, we first determined groups of regions, which were functionally connected. To this end, the average intensity traces of all regions were cross-correlated. Pairs of regions with a cross-correlation higher than 70% were assorted in a common group. Subsequently, the delay in between the regions of a specific group was corrected by cross-correlating their average intensity traces. Figure S2b shows the resulting activity propagation corrected for the signal delay in between the regions. Here, the outer regions were assorted in a common group while the center region displayed non-correlated activity. In order to include this information in the plot, the groups of correlating regions were colored as follows. Due to practical reasons, the definition of the pixels' color was performed in the Hue-Saturation-Value (HSV) color space. In this color space, a color is specified by its hue (determining the actual color), its saturation (where a relative value of 0 refers to white and a relative value of 1 to the full color), and its value (where a relative value of 0 refers to black and a relative value of 1 to the full color). In order to distinguish individual groups of correlated regions each group was assigned a specific hue value (i.e. red, green, etc.). Subsequently, the delay values were then mapped to a scale ranging from a value of 0 and a saturation of 50% (i.e. the corresponding color mixed with 50% black) to a value of 50% and a

saturation of 100% (i.e. the corresponding color mixed with 50% white). The resulting plots (compare Figure 4) thus display correlating regions in the same color, while the signal propagation in area of the same color is displayed by the color's "brightness".

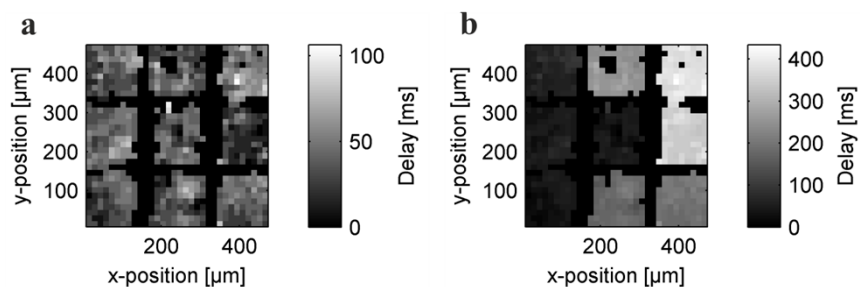


Figure S2: Ca²⁺ propagation analysis. **(a)** By correlating each pixel's intensity trace with the average trace of the corresponding region, the propagation inside the region can be detected. **(b)** The signal delay between the individual regions can be detected by cross-correlating the average traces of the individual regions and shifting correlating groups of regions to a common time scale. In this case, the center region's activity is not correlated with that of the outer regions. It represents its own group of regions with an independent time scale starting at 0 ms.

2. Frequency analysis

Besides the Ca²⁺ propagation patterns, the periodicity of the Ca²⁺ signal was evaluated. To this end, the power spectral density (PSD) of the average intensity trace of every region, as well as the time between the individual peaks (i.e. the interspike interval) and its standard deviation were calculated. Figure S3 shows a propagation plot of a sample, as well as a bar plot of the averaged interspike intervals of all regions and two exemplary PSDs. For descriptive purposes, the regions in Figure S3a were labelled with numbers. The average interspike interval for region 6 clearly deviates from the value for the other regions. A comparison of the standard deviations also shows a different value for this region (see Fig. S3b). This indicates a different frequency as well as a different periodicity for the signal of region 6 compared with the other regions.

Figures S3c and d show exemplary PSDs for regions 1 and 6, respectively. It can be seen that the intensity of the individual peaks is lower for region 6 than for region 1 and the peaks appear at a lower frequency. Furthermore, the amount of noise is higher for region 6. In agreement with

the bar plot shown in Figure S3b, this indicates a lower frequency and a lower periodicity for region 6.

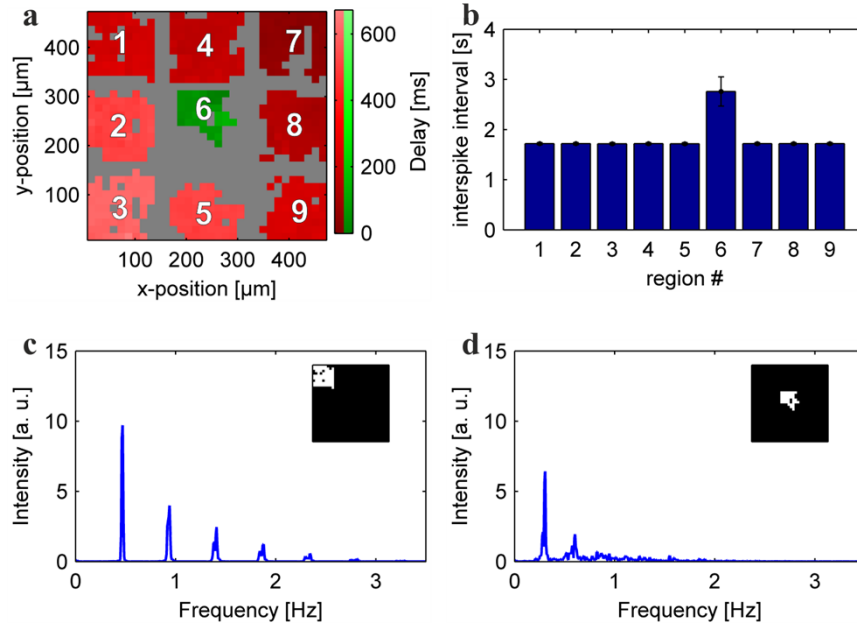


Figure S3: Frequency analysis of the Ca^{2+} imaging data. **(a)** Propagation plot of the sample prepared as described above. In addition, the individual regions were labelled with numbers. **(b)** Bar plot of the interspike intervals of the individual regions as labelled in **(a)** (error bars: standard deviation). Compared with the other regions, region 6 shows a clearly distinct average interspike interval with a larger standard deviation. **(c)** and **(d)** Power spectral densities (PSD) of region 1 and 6, respectively. The inlays show logical masks of the corresponding regions. The PSD of region 1 shows less noise and a higher intensity than the PSD of region 6. Furthermore, the main peak appears at a lower frequency. In agreement with the interspike intervals shown in **(b)**, this shows that region 6 displays a less periodic signal with a lower frequency.

3. Peripheral coupling

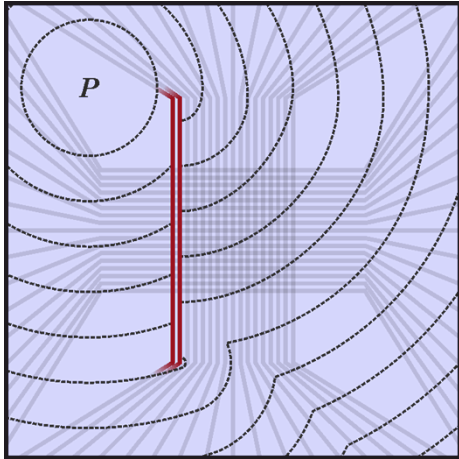


Figure S4: Schematic illustrating the peripheral coupling in the HL-1 layers. In the center of the chip, the wires have a width of $10\ \mu\text{m}$. Thus, the dissipation of electrical power and consequently the heating is highest in this area (indicated in red). In the peripheral regions of the chip, the wires widen to meet the contact pads (compare Figure 1b). The heating in these areas is thus limited. For a given pacemaker position (indicated as P), the Ca^{2+} signal can thus travel around the actual lesion and occur on both sides. In this case, a successful lesion can be detected by a phase shift and/or a change in propagation direction on both sides of the lesion.

4. Simulated temperature profiles

In addition to the thermal profiles determined by FLIM measurements, finite element simulations of an equivalent 2D system were performed. In this case, the lower set of wires was neglected and only the upper set of wires embedded in a polyimide layer on top of an oxidized silicon wafer was simulated. Underneath the silicon wafer, a block of aluminum simulating the chip holder's thermal capacity was included. The medium on the chip was assumed to be water. The power density dissipated in the thin part of the wire is calculated as follows. For our specific chip geometry, the contribution of the thin part of the wire (i.e. not the feedlines) to its overall resistivity can be calculated to amount to approximately 46%. Thus, 46% of the electrical power in the wire can be assumed to dissipate in the thin part. Figure S5a shows thermal profiles at the chip's surface simulated for varying electrical power applied to two neighboring wires (x-axis corresponds to that of Figure 2). Figure S5b shows the maximum temperatures reached depending on the power applied to two neighboring wires.

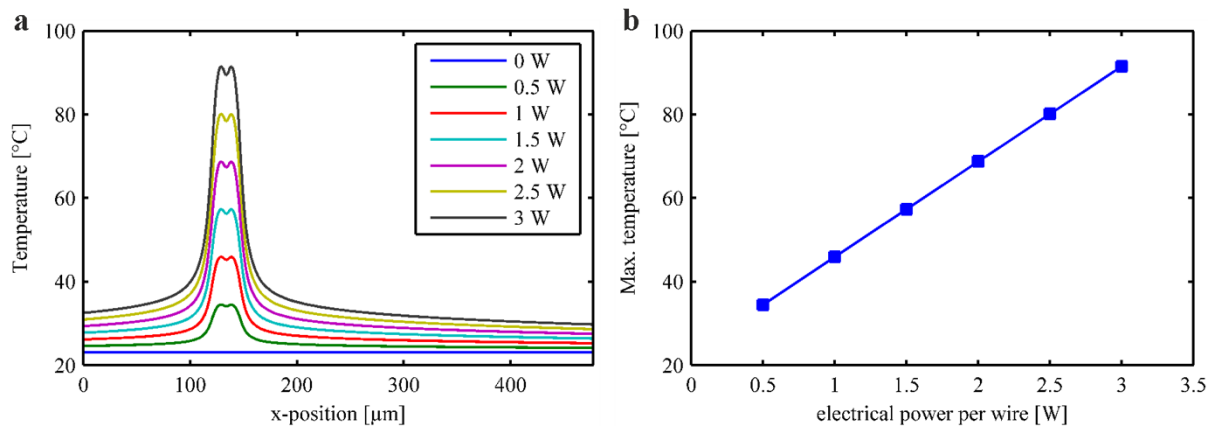
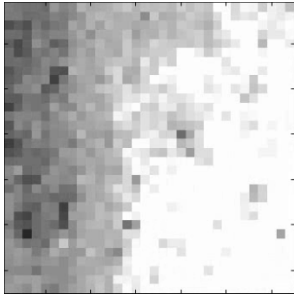


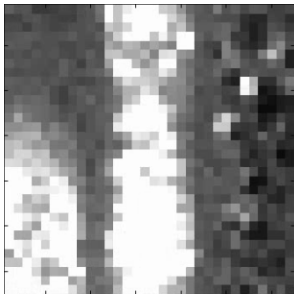
Figure S5: Simulated thermal profiles at the chip's surface. **(a)** Temperature at the chip's surface in dependence of the x-position and the electrical power applied to two neighboring wires. In correspondence to Figure 2, the wires are located at approximately $x = 126 \mu\text{m}$ and $x = 140 \mu\text{m}$. **(b)** Maximum temperature at the chip's surface depending on the electrical power applied to the two wires. A clear linear dependence can be seen.

5. Information to supplementary videos 1-3



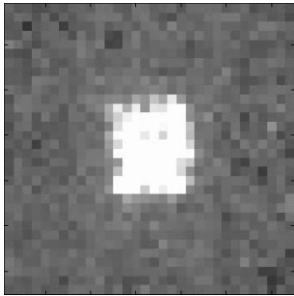
Supplementary video 1

- Recorded at an exposure time of 30.5 ms (approx. 32.8 fps) using a sequential subtraction of 4 frames and a rolling average of 4 frames
- Video shows the data in real time after downsampling to 32x32 pixels and filtered with a 300 ms Gaussian filter.



Supplementary video 2

- Recorded at an exposure time of 8.19 ms (approx. 122 fps) using a sequential subtraction of 4 frames and a rolling average of 4 frames
- Video shows the data in real time after downsampling to 32x32 pixels and filtered with a 300 ms Gaussian filter.



Supplementary video 3

- Recorded at an exposure time of 8.19 ms (approx. 122 fps) using a sequential subtraction of 4 frames and a rolling average of 4 frames
- Video shows the data in real time after downsampling to 32x32 pixels and filtered with a 300 ms Gaussian filter.

In order to reduce the file size, all videos were converted to a frame rate of 30 fps by discarding excess frames. Additionally, all videos were compressed using xvid compression.